Available online at www.sciencedirect.com
ScienceDirect
Ceramics International 34 (2008) 1875–1883
CERAMICS INTERNATIONAL
www.elsevier.com/locate/ceramint

Codoped Cr and W rutile nanosized powders obtained by pyrolysis of triethanolamine complexes

Soumya K. Biswas, A. Pathak, N.K. Pramanik, D. Dhak, P. Pramanik *

Department of Chemistry, Indian Institute of Technology Kharagpur, Kharagpur 721302, India

Received 12 October 2006; received in revised form 5 April 2007; accepted 1 July 2007
Available online 10 August 2007

Abstract

Polycrystalline, rutile phase, nanosized mixed transition metal oxide, with compositions $Cr_{2x}W_xTi_{1-3x}O_2$ ($x = 0.05$, 0.1, 0.15), have been prepared through pyrolysis of aqueous precursor solutions containing stoichiometric amounts of ammonium dichromate, dimethylammonium tungstate, titanium oxalate and optimum amounts of TEA. The rutile phased oxide solid solutions obtained on calcination of the precursors at 800 °C have been characterized by XRD, TG-DTA, BET surface area measurement, UV–visible spectroscopy and TEM. Substitution of Cr(III) for Ti(IV) ions in the rutile lattice causes colouring effect in the solid solutions while the W(VI) ions are incorporated for charge compensation. The nanosized powders of the solid solutions exhibit buff colour and their average particle sizes and specific surface areas are found to range between 30–60 nm and 56–68 m^2/g, respectively. Various TiO_2-based mixed oxides of variant colours can be prepared through the developed chemical process.

Keywords: D. Transition metal oxides; Rutile phase; Cr–W–Ti–O; Nanosize; Chemical method

1. Introduction

Incorporation of chromophorous transition metal ions, having ionic radii similar to Ti^{4+} (0.605 Å), into the host rutile (TiO_2) lattice normally generates oxide solid solutions with stable colorimetric properties. In formulations such as: $Ti^{IV}(A^{V(VI)}B^{II(III)})O_2$ [1–5], the colouring effect is produced when the Ti(IV) ion, which is surrounded by six neighbouring oxygen atoms at the corners of a regular (but slightly distorted) octahedron in the rutile lattice, is substituted by transition metal ions of lower valency at the 'B' site (e.g., $B = Cr^{3+}$; ionic radius = 0.615 Å) while the higher valency ions at the 'A' site (e.g., $A = W^{6+}$; ionic radius = 0.60 Å) compensate for the charge off set, such that their molar ratios ensure an overall electroneutrality in the oxide solid solutions.

In recent years, chromium(III)-doped rutile phased titanium dioxide solid solutions have gained considerable recognition [6,7] as durable, chemical resistant inorganic pigments with stability [8] beyond 1000 °C. Doping titanium dioxide with Cr^{3+} ions greatly reduces its tendency to act as a photocatalyst [9], making the oxides extremely resistant to chalking. Alfred et al. [10] studied the electronic properties of TiO_2 catalysts doped with different amounts of Cr_2O_3 and WO_3 and discussed the structural defects therein. The preparation of these solid solutions have mainly been reported through solid-state reactions [2–5], which require several processing steps such as, initial ball milling of the raw materials (usually metal oxides and/or salts) for homogenization; calcinations of these mixtures at high temperature (1100–1200 °C) to obtain the desired crystalline phases and colours; and finally, wet milling to the reduce particle size. The solid-state method usually results in coarse-grained and agglomerated particles.

Solution-based chemical methods of preparation of the oxide solid solutions in contrast are attractive alternative to the conventional solid-state synthesis technique. They not only have the advantage of reduced processing steps but also ensure a precise control of composition and stoichiometry in multi-component formulations, phase purity in the final product, and better control of particle size in the final powders through molecular level mixing of the starting compounds in a solution. Uniformly distributed particles [11] with average grain sizes

* Corresponding author. Tel.: +91 3222 283322; fax: +91 3222 255303.
E-mail addresses: pramanik@chem.iitkgp.ernet.in, panchanan_123@yahoo.com (P. Pramanik).

0272-8842/$34.00
doi:10.1016/j.ceramint.2007.07.014

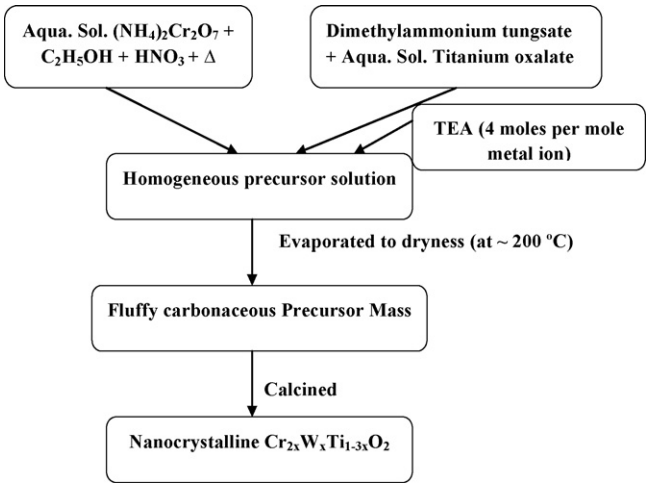

Fig. 1. Process for the preparation of the nanosized solid solution compositions of $Cr_{2x}W_xTi_{1-3x}O_2$.

less than 100 nm obtained through the solution-based methods. In spite of the said advantages, there have been only a few literature reports on the preparation of Cr(III)- and W(VI)-doped rutile-based oxide solid solutions through aqueous solution-based chemical methods so far, because of the diverse solubilities of the constituent ions and also due to scarcity of water-soluble salts of titanium and easy hydrolysis of the available ones. In this paper we report the preparation of Cr(III)-doped rutile-based oxide solid solutions with compositions $Cr_{2x}W_xTi_{1-3x}O_2$ (where $x = 0.05, 0.10, 0.15$) through low temperature thermolysis of precursors obtained through evaporation of aqueous based precursor solutions comprising of soluble complexes of the constituent metal ions and optimum amounts of triethanolamine (TEA) [12]. The use of a water-soluble complex of tungstate (i.e., dimethylammonium tungstate) as the source of tungstate ions, and the formation of water-soluble complexes of Ti(IV) and Cr(III) with TEA in solution helps to retain the constituent metal ions in the precursor solution and prevents their hydrolysis and segregation/precipitation during the processing. The method is simple, the processing temperature required is much lower than those reported in the literature, and the final product consists of nanosized particles with relatively narrow distribution in sizes. The present method is better than a coprecipitation method because, the synthesis of multi-component complex-systems like Cr- and W-doped titanium oxides by simple coprecipitation method does not produce nanosized materials maintaining the stoichiometry in the products.

2. Experimental

Raw materials used: (a) ammonium dichromate (Merck India Ltd.), (b) sodium tungstate (Merck India Ltd.), (c) titanium(IV) oxide (Merck India Ltd.), (d) oxalic acid dihydrate (Merck India Ltd.), (e) TEA (Merck India Ltd.), (f) diammonium oxalate monohydrate (Merck India Ltd.), (g) HCl (35%) (Merck India Ltd.), (h) HNO_3 (70%) (Merck India Ltd.), (i) NH_4OH (25%) (Merck India Ltd.), (j) HF (48%) (Merck India Ltd.).

Cr(III)-doped rutile-based oxide solid solutions with compositions $Cr_{2x}W_xTi_{1-3x}O_2$ (where $x = 0.05, 0.1, 0.15$) were prepared using freshly prepared aqueous stock solutions of ammonium dichromate, dimethylammonium tungstate[1], titanium oxalate[2] and TEA. Required volume of the aqueous solution of ammonium dichromate (0.1 M) was first taken from a freshly prepared stock and heated in presence of ethanol and few drops of concentrated nitric acid to have the colour of the solution changed from orange to bluish green, as Cr(VI) got reduced to Cr(III). Appropriate volumes of the aqueous solutions of titanium oxalate and dimethylammonium tungstate were then taken from their respective stocks as per the required stoichiometries and added to the bluish green solution of Cr(III) under constant stirring. Finally, optimum amount of TEA was added into the solution mixture to keep the metal ions in solution through complexation and the pH of the solution was adjusted to ~5 with the help of nitric acid to avoid precipitation. The amount of TEA was always kept in excess to the total cations present in the solution mixture (i.e., ~4 mol with respect to the total moles of the metal ions). The resultant precursor solution was homogenized by constant stirring and eventually set to evaporate by heating at ~200 °C. On complete dehydration of the precursor solution, the TEA and the metal-complexes decomposed with the evolution of dense fumes and resulted in a voluminous, fluffy, black organic-based mass. The fluffy carbonaceous mass was crushed to obtain the fine precursor powders, the rutile phased solid solutions were eventually obtained through calcination of the fine powders for 2 h at temperatures ranging between 450 °C and 800 °C using alumina crucible, maintaining a heating rate of 10 °C/min in ambient atmosphere. Flow-chart of the process is depicted in Fig. 1.

[1] *Preparation of aqueous solution dimethylammonium tungstate*: weighed amounts of sodium tungstate was dissolved in deionized water and then it was added drop wise into dilute hydrochloric acid (>5N) to obtain a yellow precipitate of water insoluble tungstic acid. The pH of the medium was maintained at ~2. The precipitate was filtered and after washing with deionized water to remove the chloride ions it was dissolved in minimum volumes of dimethylamine (40% solution) and finally the resultant solution was diluted to the required volume with deionized water to obtain the stock of dimethylammonium tungstate solution. The tungsten-content in the solution was confirmed by assay process.

[2] *Preparation of aqueous solution of titanium oxalate*: aqueous solution of titanium oxalate was prepared starting from its hydrous oxide [$TiO_2 \cdot nH_2O$]. To begin with, weighed amounts of titanium dioxide (TiO_2) (1 M, >99%) was dissolved in 48% HF (>7 M) by heating over a water bath for 28/30 h to obtain a clear solution of the titanium-fluoride complex [TiF_6^{2-}]. Hydrous titanium oxide was then precipitated out from this clear solution by drop wise addition of dilute ammonia, and the precipitate was washed with 5% ammonia to make it free from fluoride ions. The precipitate was then slowly dissolved in an aqueous mixture of equal volumes of oxalic acid (0.1 M) and ammonium oxalate (0.1 M) with constant stirring to obtain a clear solution, which was diluted to the required volume with deionized water to get the stock solution of titanium oxalate. The aqueous mixture of oxalic acid and ammonium oxalate used for the dissolution was freshly prepared and always used in excess to stoichiometric requirement of two moles per mole of Ti(IV) ion. The titanium content in the solution was estimated by the assay method.

The phase identification in the oxide solid solutions was performed using room temperature X-ray powder diffraction (XRD) (Philips X-ray Diffraction Unit, PW 1710) with Cu Kα radiation (λ = 1.5406 Å) and Ni filter. In the XRD studies, the powders obtained at different heat treatment temperatures were mounted in the sample holder and recorded in the 2θ ranges from 20° to 70°. The X-ray diffraction lines were analyzed using PCPDFWIN. The crystallite size (D) and the effective strain (η) in the solid solution compositions were calculated from the full widths at half maximum (FWHM) of the diffraction peaks (2θ range = 15°–65°; step = 0.025°; sampling time = 10 s) after introducing the correction for instrumental broadening using standard silicon. The FWHM were expressed by the following equations [13] considering the peaks to be of the Gaussian type

$$(\beta^0)^2 = (\beta^m)^2 - (\beta^s)^2$$

and

$$\frac{\beta^0 \cos\theta}{\lambda} = \frac{1}{D} + \frac{\eta \sin\theta}{\lambda}$$

where β^0 is the integral of FWHM; β^m the FWHM considering the particle size effect; β^s the FWHM due to instrumental effect, for the standard Si; θ the half incident angle of the X-ray and λ is the wavelength of the target material (λ = 1.5406 Å). The crystallite sizes (D) and the effective strains (η) in the powder samples were respectively obtained from the intercept at $x = 0$ and the slope of the best-fit line plot of ($\beta^\circ \cos\theta/\lambda$) versus ($\sin\theta/\lambda$). The fraction of rutile phase formed in the calcined samples was calculated from the Spurr equation [14]

$$F_R = \frac{1}{1 + 1.26\,(I_A(1\,0\,1)/I_R(1\,1\,0))}$$

where F_R is the mass fraction of rutile phase in the samples and I_A (1 0 1) and I_R (1 1 0) are the intensities of d_{101} and d_{110} lines of the anatase and rutile phase, respectively. Simultaneously recorded thermogravimetric, differential thermogravimetric and differential thermal analysis (TG/DTG/DTA) of the precursor powders were carried out in air at a heating rate of 5 °C/min using Perkin–Elmer instruments (Pyris Diamond TG/DTA). The high-resolution transmission electron microscopy (HRTEM) measurements were carried out with 200 keV electron beam using JEOL 2010 (ultrahigh-resolution model). For the HRTEM experiment, the samples were prepared by suspending the heat-treated powder in ethyl alcohol by sonication and taking a drop of the suspension on 200-mesh carbon coated copper grid. Particle size distributions of both the samples were determined by using the UTHSCSA Image Tool program (version 3.00) using three TEM images. The BET specific surface areas of the calcined powders (after out-gassing the powders at 150 °C for 4 h) were determined through N_2 adsorption isothermal at 77 K using Beckman Coulter SA3100 surface area analyzer. The colour of the powders was assessed from CIEL*a*b* colour parameter measurements, calculated from the diffuse reflectance spectra taken with a Perkin–Elmer colorimeter using a standard illuminant D. According to the method the parameter L* represents the brightness of a sample; L* is a lightness axis [black (0) to white (1 0 0)]; a* represents the green (−) → red (+) axis and b* the blue (−) → yellow (+) axis.

3. Results and discussion

The thermal studies of the carbonaceous precursors for the composition $Cr_{2x}W_xTi_{1-3x}O_2$ ($x = 0.05$) are depicted in Fig. 2. The DTA curves for all the precursor compositions revealed a broad exothermic thermal affect between 250 °C and 470 °C

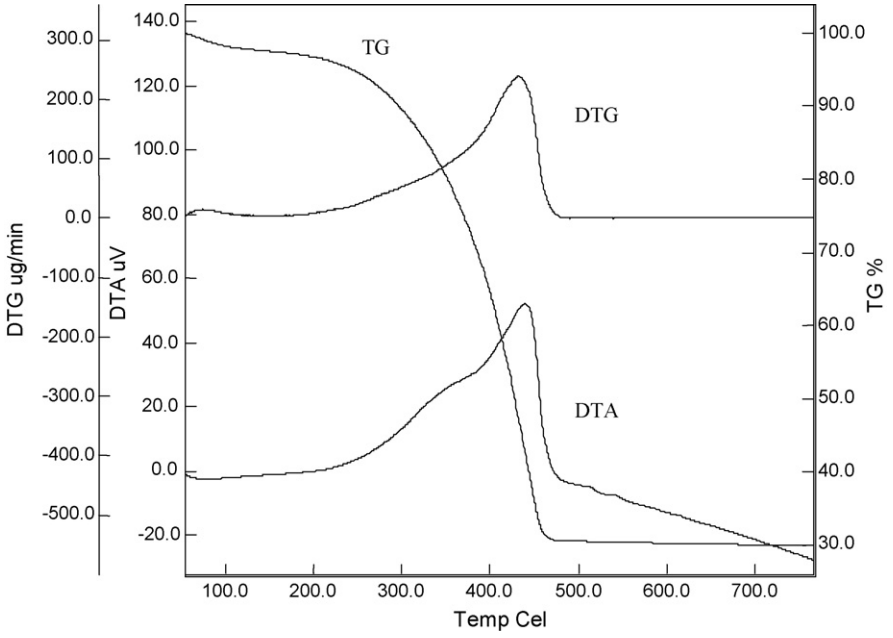

Fig. 2. Simultaneously recorded TGA/DTG/DTA plots of the carbonaceous precursors of $Cr_{2x}W_xTi_{1-3x}O_2$ ($x = 0.05$) solid solution composition.

with their respective peak positioned around 445 ± 10 °C. This exothermic affect may be attributed to the oxidation of the organic remnants from the decomposed metal-complexes and TEA present in the carbonaceous precursors. The entire thermal affect was accompanied by evolution of large amounts of gases—such as, water vapour, CO, CO_2, NO_2, etc., which was manifested by a sharp, single step weight loss in the TG curve (around 70%) and a single peak in the DTG curve. The TG curves in Fig. 2 shows that the weight loss from the amorphous precursor powders continued beyond the peak temperatures of the exothermic affect revealing that samples were not completely carbon free at around 445 ± 10 °C. Crystallization of the oxide phase (i.e., formation of the oxide solid solution) was not very clearly visible from the DTA curve however, a small kink in the curve at around 500 °C, without any visible weight loss in the TG/DTG curves, may be attributed to it. The phase transformation from anatase to rutile form was not detectable from DTA curves because of the small and gradual changes involved.

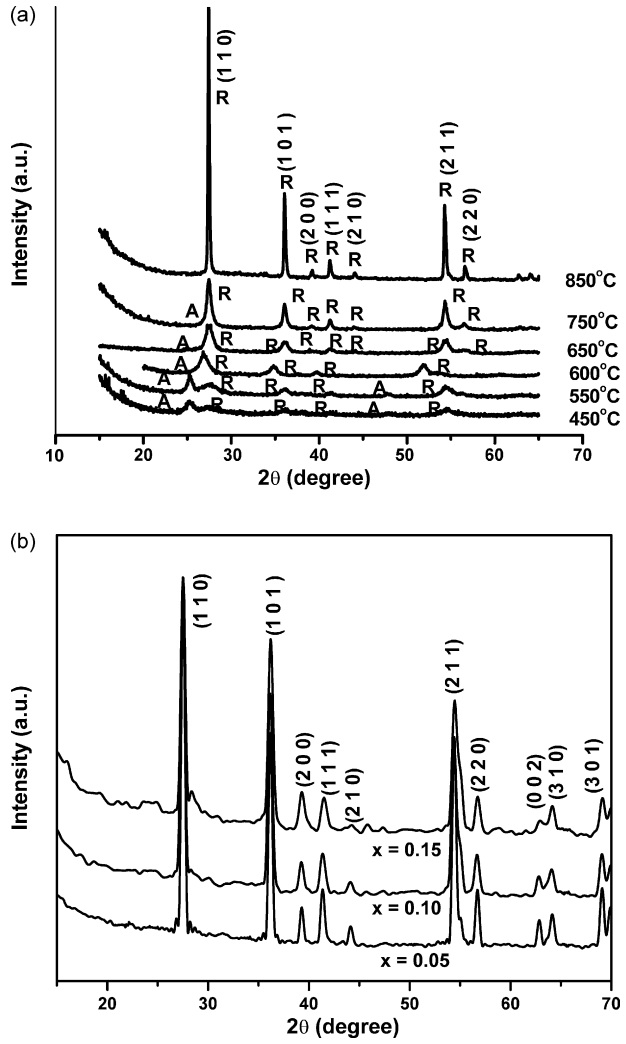

Fig. 3. (a) X-ray diffractograms (using Cu Kα radiation) of the $Cr_{2x}W_xTi_{1-3x}O_2$ ($x = 0.05$) precursors on calcination at various temperatures. (b) X-ray diffractograms (using Cu Kα radiation) of the various $Cr_{2x}W_xTi_{1-3x}O_2$ solid solution compositions after calcination at 800 °C/2 h.

Fig. 3a shows the characteristic X-ray powder diffraction (XRD) patterns for the $Cr_{2x}W_xTi_{1-3x}O_2$ ($x = 0.05$) precursor powders, when heat-treated at various temperatures between 450 °C and 800 °C for 2 h. The virgin precursors were amorphous to X-ray and crystallization of the oxide phase began at calcination temperatures higher than 450 °C, which was reflected by the emergence of broad, low-intensity diffraction lines corresponding to the anatase (d_{101}) and rutile (d_{110}) phases. At calcination temperature of 550 °C (2 h), the intensities of the d_{101} and d_{110} lines, corresponding to the anatase and the rutile phase, respectively, were comparable. Increase in the heat-treatment temperatures to 600 °C (and beyond) resulted in crystal growth and increase in the rutile fraction in the samples, which was evident by gradual sharpening of the diffraction lines, and increase in the intensity of the d_{110} lines corresponding to the rutile phase and diminishing of the d_{101} corresponding to the anatase phase. The percentages of the rutile phase; the relative intensities of the XRD peaks corresponding to the anatase and the rutile phases in the $Cr_{2x}W_xTi_{1-3x}O_2$ ($x = 0.05$, 0.1 and 0.15) compositions at various heat-treated temperatures are tabulated in Table 1 along with the tap densities for $x = 0.05$ composition. On calcination of the precursors at 750 °C/2 h, the percentage of the rutile phase in $Cr_{2x}W_xTi_{1-3x}O_2$ ($x = 0.05$) was found to be around 96%, and the pure rutile phase was obtained at the calcination temperatures of 800 °C/2 h. The XRD peaks for the various solid solution compositions were indexed using the standard data available for the rutile phase (JCPDS card no. 781510) and the same have been shown in Fig. 3b. It was observed that the precursors of the oxide solid solution with $x \geq 0.2$, the formation of the rutile phase was accompanied by the phase of Cr_2O_3 when the heat-treatment of the compositions were carried out between 650 °C and 900 °C. Prolonging the heat-treatment period (for 20–30 h) at higher temperatures (1300–1400 °C) eventually resulted in the pure rutile phase in these precursors (i.e. for $x \geq 0.2$) however. This was accomplished at the expense of loss of the nanocrystallinity in the sample.

It can be thus inferred that the metastable anatase phase (typically preserves a large surface area) underwent transformation to the rutile phase on calcination between 550 °C and 800 °C. At calcination temperatures above 550 °C, a more rapid phase transformation from anatase to rutile was observed for $x = 0.10$ and 0.15 compositions. The crystallite sizes (D, as calculated from FWHM of the XRD lines) and corresponding surface areas for the calcined (800 °C/2 h) $Cr_{2x}W_xTi_{1-3x}O_2$ ($x = 0.05$, 0.10, 0.15) compositions are shown in Table 2. Fig. 4 shows the plot of ($\beta^0 \cos\theta/\lambda$) versus ($\sin\theta/\lambda$) for the typical solid solution composition with $x = 0.05$, the effective strain (η), obtained from the slope of the plot, was found to be 0.00243.

The lattice parameters (i.e., a and c) for the calcined (800 °C/2 h) rutile phase $Cr_{2x}W_xTi_{1-3x}O_2$ solid solutions, which were calculated following the reflection planes (2 0 0) and (0 0 2), have been tabulated in Table 3. These calculated values of a and c were found to be in close agreement with those reported for the standard rutile phased TiO_2 (JCPDS data card no.781510). As there was no evidence of any additional phase

Table 1
Percentage of rutile phase, relative XRD intensities of the anatase and rutile phases and tap densities of the various $Cr_{2x}W_xTi_{1-3x}O_2$ compositions at different calcination temperatures

Calcination temperature (°C/2 h)	Rutile phase (%) for compositions			XRD intensities of the A and R phases for compositions[a]			Tap densities (g/cm^3)
	$x = 0.05$	$x = 0.10$	$x = 0.15$	$x = 0.05$	$x = 0.10$	$x = 0.15$	$x = 0.05$
550	41.0	72.4	75.2	A (s), R (w)	A (mw), R (s)	A (mw), R (s)	0.1325
650	85.8	90.2	92.8	A (mw), R (s)	A (w), R (s)	A (w), R (s)	0.1633
750	96.1	98.3	98.0	R (s), A (vw)	R (s), A (vw)	R (s), A (vw)	0.1758
800	100.0	100.0	100.0	R (s)	R (s)	R (s)	0.2345

[a] Relative XRD intensities of the anatase (A) and rutile (R) phases; s = strong, w = weak, mw = medium weak, vw = very week.

Table 2
Variation in crystallite size, surface area and particle size for calcined (at 800 °C for 2 h) $Cr_{2x}W_xTi_{1-3x}O_2$ solid solution with change in dopant concentration

Composition of $Cr_{2x}W_xTi_{1-3x}O_2$	Crystallite size (nm) (±2 nm)[a]	BET surface area (m^2/g)	TEM particle size (nm) (±5 nm)[b]
$x = 0.05$	30	60	40.0
$x = 0.10$	32	56	45.0
$x = 0.15$	35	58	38.0

[a] Crystallite size calculated from FWHM of the X-ray diffraction peaks.
[b] Average of the smallest visible isolated particle/crystallite agglomerate as observed from TEM studies for the respective compositions.

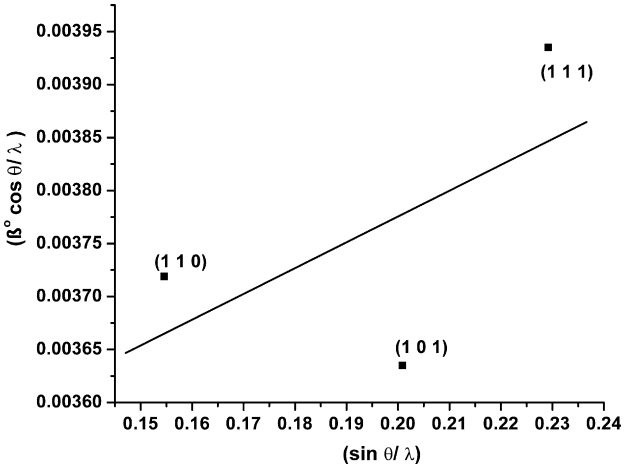

Fig. 4. Plot of ($\beta^{o}\cos\theta/\lambda$) vs. ($\sin\theta/\lambda$) for evaluating crystallite size and strain from FWHM of the X-ray diffraction peaks for $Cr_{2x}W_xTi_{1-3x}O_2$ (with $x = 0.05$) solid solution composition.

in the samples, that were calcined at 800 °C, and also because the unit-cell parameters fairly matched with the chemical composition, therefore the structure of $Cr_{2x}W_xTi_{1-3x}O_2$ solid solutions (calcined at 800 °C) was confirmed to be of purely rutile type. Increase in the lattice parameters a and c, with increasing fraction of Cr(III) [i.e., from $x = 0.05$ to $x = 0.15$] in the solid solution $Cr_{2x}W_xTi_{1-3x}O_2$, caused by substitution of the Ti^{4+} ions ($r = 0.605$ Å) by Cr^{3+} and W^{6+} ions followed the Vegard's law [15].

The finer morphological details of the calcined (800 °C/2 h) solid solution samples and their size distributions were studied using transmission electron microscopy (TEM). The smallest visible particles in the bright field electron micrograph can be identified as single crystallites and/or their aggregates. Fig. 5a and b depict the TEM micrographs for the calcined (800 °C/2 h) $Cr_{2x}W_xTi_{1-3x}O_2$ ($x = 0.05$ and 0.10) solid solution compositions, respectively. It was observed that the particles were almost spherical with average particle diameters ranging between of 30 nm and 60 nm. The distribution in particle sizes, evaluated from TEM studies, for the same samples are shown through bar charts in Fig. 5c and d, respectively. Selected-area electron diffraction (SAED) pattern of the calcined (800 °C/2 h) $Cr_{2x}W_xTi_{1-3x}O_2$ ($x = 0.05$) composition (Fig. 5e) showed distinct rings corresponding to the (1 1 0), (1 0 1), (1 1 1), (2 1 1) planes in a rutile lattice, thus inferring the powders to be small agglomerates of nanosized polycrystallites having the rutile structure. HRTEM image for the same sample in Fig. 5f depicted the finer details in their crystal structure. Lattice spacing of about 3.22 Å between the adjacent lattice planes, as examined from the HRTEM image, corresponded to the distance between (1 1 0) crystal planes in the rutile structure, as the crystals were oriented along the (1 1 0) plane.

Table 3
Variation in lattice parameters (a, c) and volume (at 800 °C for 2 h) $Cr_{2x}W_xTi_{1-3x}O_2$ solid solution with change in dopant concentrations

Composition of $Cr_{2x}W_xTi_{1-3x}O_2$	Lattice parameter (a) (Å)	Lattice parameter (c) (Å)	Volume (Å^3)	c/a
$x = 0.05$	4.583 ± 0.004	2.955 ± 0.003	62.05 ± 0.02	0.6447
$x = 0.10$	4.586 ± 0.002	2.956 ± 0.002	62.15 ± 0.01	0.6445
$x = 0.15$	4.589 ± 0.003	2.956 ± 0.005	62.26 ± 0.02	0.6441

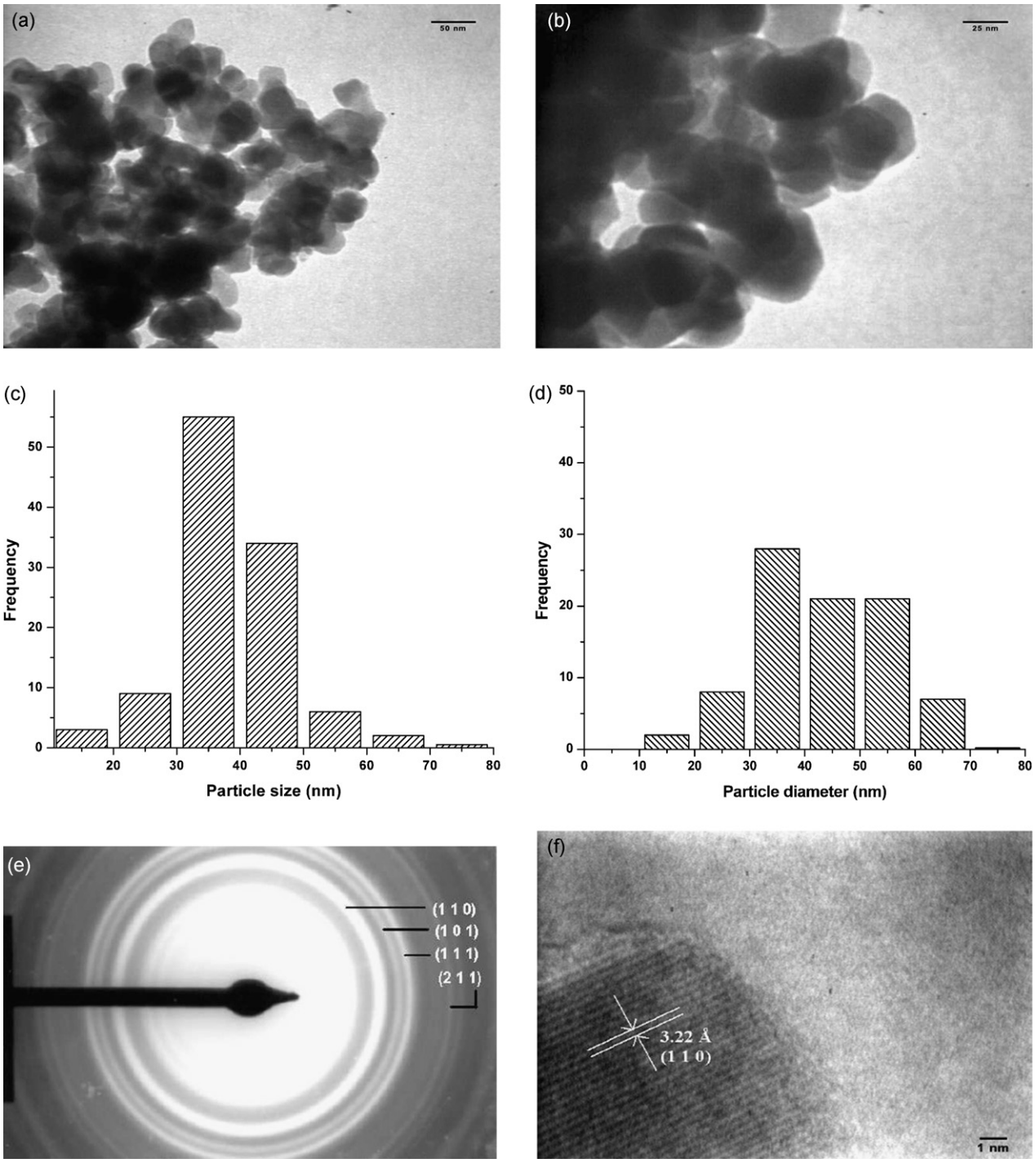

Fig. 5. (a) Bright field TEM micrograph of the calcined (800 °C/2 h) $Cr_{2x}W_xTi_{1-3x}O_2$ ($x = 0.05$) solid solution composition. (b) Bright field TEM micrograph of the calcined (800 °C/2 h) $Cr_{2x}W_xTi_{1-3x}O_2$ ($x = 0.10$) solid solution composition. (c) Distribution of particle sizes, evaluated from TEM studies, for the calcined (800 °C/2 h) $Cr_{2x}W_xTi_{1-3x}O_2$ ($x = 0.\ 05$) solid solution composition. (d) Distribution of particle sizes, evaluated from TEM studies, for the calcined (800 °C/2 h) $Cr_{2x}W_xTi_{1-3x}O_2$ ($x = 0,\ 10$) solid solution composition. (e) Selected-area electron diffraction (SAED) pattern of the calcined (800 °C/2 h) $Cr_{2x}W_xTi_{1-3x}O_2$ ($x = 0.05$) composition showing distinct rings corresponding to the (1 1 0), (1 0 1), (1 1 1), (2 1 1) planes in a rutile lattice. (f) HRTEM image of the calcined (800 °C/2 h) $Cr_{2x}W_xTi_{1-3x}O_2$ ($x = 0.05$) composition.

The UV–visible absorption spectra for the calcined (at 800 °C/2 h) $Cr_{2x}W_xTi_{1-3x}O_2$ solid solutions, shown in Fig. 6 revealed a wide absorption band ranging from 250 nm to 850 nm in all the samples, with three distinct humps positioned at 330–340 nm, 425–470 nm and 590–640 nm, corresponding to the three respective spin allowed d–d transitions from the Cr^{3+} ions in octahedral environment. Ti^{4+} ion in titanium dioxide, being a $3d^0$ system, has no 3d-electrons for d–d electronic transition and hence appears as a white powder with no absorption in the visible range (Fig. 6). According to crystal field theory [16], bulk Cr_2O_3 samples with Cr^{3+} ion ($3d^3$ electronic configuration) in an octahedral environment is

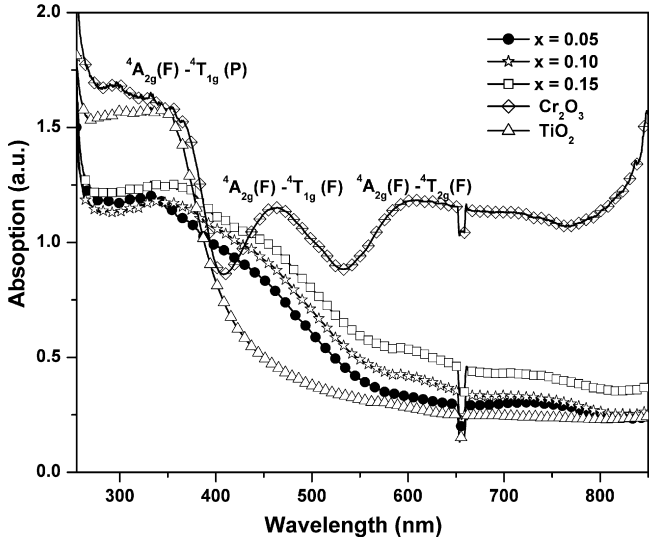

Fig. 6. UV–visible absorption spectra for calcined (at 800 °C/2 h) powders of the $Cr_{2x}W_xTi_{1-3x}O_2$ solid solution compositions.

predicted to have three absorption bands assigned to three electronic spin allowed transitions of $[^4A_{2g}(F) \rightarrow {}^4T_{2g}(F)]$ at 600 nm; $[^4A_{2g}(F) \rightarrow {}^4T_{1g}(F)]$ at 455 nm; and $[^4A_{2g}(F) \rightarrow {}^4T_{1g}(P)]$ in the UV region (Fig. 6). The energies of the first two electronic spin allowed transitions exist in the visible light energy range [17] while the third transition lies is in the ultraviolet range and therefore does not affect the colour of the samples. Observed shifts in the absorption bands of the Cr^{3+} ions in $Cr_{2x}W_xTi_{1-3x}O_2$ solid solutions to that of the bulk Cr_2O_3 samples may be due to deformation of the octahedral environment of the Cr^{3+} ions to lesser symmetry in the former. The Ti^{4+} ions in the oxygen octahedra in the rutile lattice is already slightly distorted and their substitution by slightly larger sized Cr^{3+} ions, for the formation of the solid solutions, may cause further deformation of the octahedra and may attribute to the shifts in the absorption bands of the Cr^{3+} ions in the solid solutions compared to those observed in the bulk Cr_2O_3 samples, where the Cr^{3+} ions exists in a symmetric octahedral environment. The broadness in the absorption spectra for the $Cr_{2x}W_xTi_{1-3x}O_2$ solid solutions may be due to existence of additional absorption bands corresponding to charge transfers between the constituent metal ions [Cr(III), Ti(IV), W(VI)], and between ligand and metal ions besides the spin allowed d–d transitions in Cr(III) ion in octahedral environment. Thus, the allowed d–d transitions of the Cr(III) get masked by the existence of absorption bands corresponding to metal–metal and metal–ligand charge transfers and their overlap in the UV–visible spectral range. Additionally, the substitution of the Cr^{3+} ions in the distorted rutile environment is also likely to contribute towards the broadness of the bands.

The particle sizes, in the three solid solution compositions, were almost in the same range (30–60 nm), thus the scattering due to the particle size can be assumed same for all the compositions. In this respect, the relation between reflectivity of the powder at $\lambda = 700$ nm and dopant concentrations x (in mole %) can be examined by plotting K/S (at $\lambda = 700$ nm) versus x, K/S for the solid powders, calculated applying the Kumelka–Munk equation [18] that can be expressed as

$$\frac{K}{S} = \frac{(1-R)^2}{2R}$$

where, K is the absorption coefficient, S the scattering coefficient and R is the decimal fractional reflectance. Since the sample powders of all compositions had almost same particle sizes, thus S can also be assumed to be invariable for all the sample powders. The plot of K/S (at $\lambda = 700$ nm) versus x in Fig. 7 shows the linearity confirming the intrusion of the dopants into the TiO_2 matrix to form the solid solutions [5].

The CIEL*a*b* measurements of $Cr_{2x}W_xTi_{1-3x}O_2$ ($x = 0.05$) solid solution heat-treated at its calcination temperature were done as a prototype. The CIEL*a*b* measurements represent a reddish brown colour of the sample (i.e. high b* (54.3) and low a* (18.6) parameters) and a light colour (L* by 67.8).

The BET surface areas for all compositions of $Cr_{2x}W_xTi_{1-3x}O_2$ solid solutions were found to lie between 56 m^2/g and 68 m^2/g. The surface areas for the various compositions of the calcined (800 °C/2 h) $Cr_{2x}W_xTi_{1-3x}O_2$ solid solution are summarized in Table 2. The tap densities, which corresponds the fluffiness of the powder, were observed to increase with increase in calcination temperatures for all the compositions of the solid solution (Table 1). This may be due to decrease in the volume of the samples brought about by the reduction of porosity on sintering of the particles at increased heat-treatment temperatures. FESEM micrograph (Fig. 8) for the calcined (800 °C/2 h) $Cr_{2x}W_xTi_{1-3x}O_2$ ($x = 0.05$) solid solution composition shows the aggregates of small particles. The individual particles show the size below 100 nm.

For studying the thermal stabilities of the solid solution compositions at high temperatures, the final powders were annealed at 1200 °C for 3 h. XRD phase analysis (Fig. 9) of the annealed powders showed no phase change thereby establishing the thermal stabilities of the solid solution compositions were stable even when subjected to heat-treatment at the temperatures of 1200 °C for 3 h. Furthermore, XRD phase

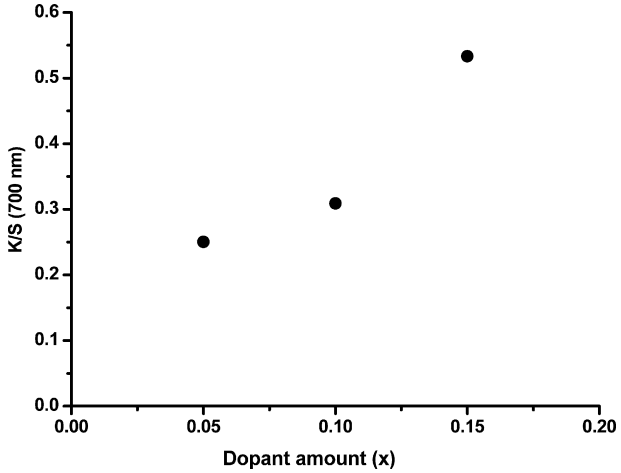

Fig. 7. Plot of K/S vs. dopant amount (x) for the various $Cr_{2x}W_xTi_{1-3x}O_2$ solid solution compositions.

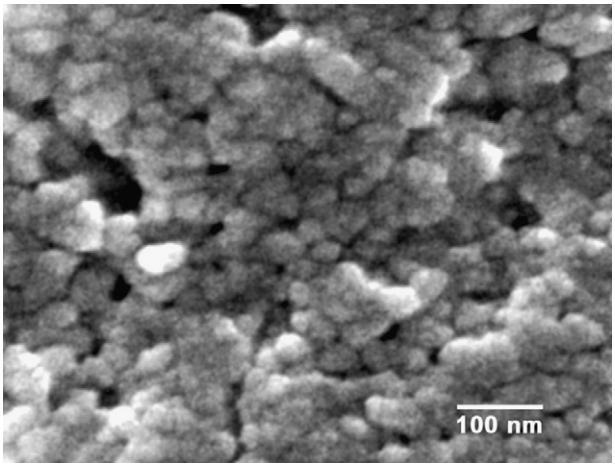

Fig. 8. FESEM micrograph of the calcined (800 °C/2 h) $Cr_{2x}W_xTi_{1-3x}O_2$ ($x = 0.05$) solid solution composition.

analysis of the powders after being subjected to treatment with dilute HCl, dilute HNO_3 and dilute NaOH were found to remain unchanged reflecting the retention of their chemical composition and colour even on post treatment thereby validating their chemical inertness under acidic and alkaline conditions.

In the developed chemical method, Cr(III)- and W(VI)-doped rutile phased TiO_2 solid solutions have been prepared by complete evaporation of aqueous based precursor solution containing stoichiometric amounts of the desired metal ions and excess of TEA. The principle was to atomistically disperse the complexed metal-ions in the polymeric network generated by the evaporation of excess triethanolamine at pH ≅ 5.

To begin with, the metal ions were homogeneously dispersed in the precursor solution through formation of stable, water-soluble coordinated complexes with TEA. Maintaining TEA in excess to the stoichiometric requirement in the precursor solution probably led to polymerization of the free amount, which provided a highly branched polymeric framework for anchoring the metal ions/metal coordinated complexes. This not only assisted in preventing segregation or, any intermittent precipitation of the metal ion from the homogeneous precursor solution during evaporation but also served as templates for the generation of a voluminous, fluffy precursor mass of metal ions embedded carbonaceous matrix on complete evaporation of the precursor solution. Slow volatilization of the carbonaceous residue in the precursor mass through calcination (at temperatures varying from 600 °C to 800 °C) in dynamic air, provided the condition for the formation of the nanoparticles of the respective mixed oxide solid solutions and facilitated the reduction of the external temperatures (800 °C) required for the formation of rutile phase through the heat provided by oxidation of carbon. The entire oxidative decomposition process was accompanied by the evolution of large amount of gases (such as: water vapour, NO_2, CO, CO_2, etc.), which helped the precursor material to dissipate the heat of combustion and thus inhibited sintering of the fine particles during the process.

Various TiO_2-based oxides of variant colours can be prepared through the developed chemical process.

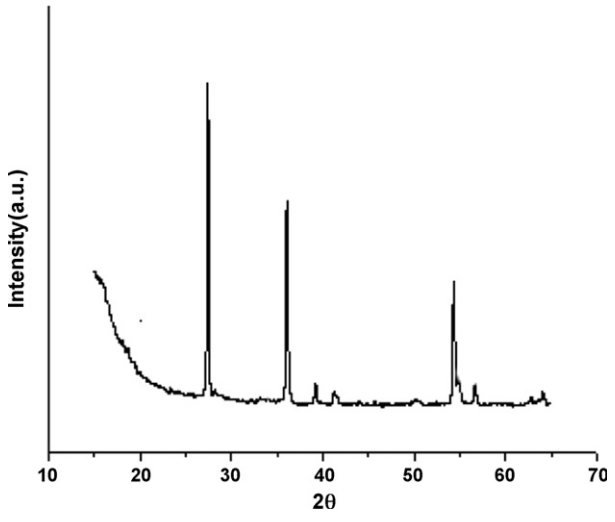

Fig. 9. XRD phase analysis of $Cr_{2x}W_xTi_{1-3x}O_2$ ($x = 0.05$) solid solution composition after annealing at 1200 °C for 3 h.

4. Conclusions

Nanosized polycrystalline rutile phase inorganic mixed oxides, with compositions $Cr_{2x}W_xTi_{1-3x}O_2$ ($x = 0.05$, 0.10, 0.15), have been prepared through an energy-efficient chemical method that is simple, has excellent control of composition and stoichiometry. The method is based on complete evaporation of aqueous based precursor solution containing excess of triethanolamine and stoichiometric amounts of the desired metal ions that are atomistically dispersed through formation of water-soluble coordinated complexes. The calcination (in dynamic air) of the carbonaceous precursors, obtained from the complete dehydration of the precursor solutions, resulted in the nanoparticles of the mixed oxide solid solution in the pure rutile phase at external temperatures as low as 800 °C for all the compositions. The particles were observed to be almost spherical having relatively narrow distribution in sizes with average diameters ranging between of 30 nm and 60 nm. The average BET surface areas were found to lie between 56 m^2/g and 68 m^2/g. The lattice parameters, a and c, of the compositions were found to increase linearly with increased dopant concentrations following Vegard's law due to substitution of the Ti(IV) ions by relatively larger mean ionic radius of two Cr(III) and W(VI) ion. Increasing the fraction of chromium contained in TiO_2 within the range $0.05 \leq x \leq 0.15$, resulted in pure rutile phase oxide solid solutions with decreasing reflectance in the visible region.

Acknowledgement

The authors express thanks to the Department of Science and Technology, Government of India, for providing the financial support for the research work.

References

[1] M.A. Tena, J. Morós, G. Carda, E. Cordoncillo, P. Escribano, J. Alarcón, Synthesis of $Cr_xTi_{1-2x}Nb_xO_2$ $0 \leq x \leq 0.5$ rutile solid solutions from alkoxides, J. Mater. Sci. 29 (1994) 3817–3821.

[2] T.P. Tavala, N.G. Brinzan, V. Florea, Red-brown pigments in the Cr_2O_3–TiO_2–WO_3 system, Revue Roumaine de Chimie 22 (5) (1977) 787–792.

[3] S. Sorlí, M.A. Tena, J.A. Badenes, J. Calbo, M. Llusar, G. Monrós, Structure and color of $Ni_xA_{1-3x}B_{2x}O_2$ (A = Ti, Sn; B = Sb, Nb) solid solutions, J. Eur. Ceram. Soc. 24 (2004) 2425–2432.

[4] E. Ramos, M.L. Veiga, R. Fernández, R. Sáez-Puche, C. Pico, Synthesis, structural characterization, and two-dimensional antiferromagnetic ordering for the oxides $Ti_{3(1-x)}Ni_xSb_{2x}O_6$ ($1.0 \geq x \geq 0.6$), J. Solid State Chem. 91 (1991) 113–120.

[5] D. Huguenin, T. Chopin, New titanium precursors for manufacture of colored pigments, Dyes Pigments 37 (2) (1998) 129–134.

[6] D.R. Swiler, J. Livingston, Mixed metal oxide "titanate" pigments, Int. Conf. Prod. Appl. Spec. Inorg. Pigments (1993) 32–45.

[7] M.A. Malati, W.K. Wong, Doping titanium dioxide for solar energy applications, Surf. Technol. 22 (4) (1984) 305–322.

[8] J. Maloney, Titanate pigments: colored rutile, priderite and pseudobrookite structured pigments, in: Hugh.M. Smith (Ed.), High Performance Pigments, Wiley-VCH, 2002, pp. 53–73.

[9] J.M. Herrmann, J. Disdier, P. Pichat, Effect of chromium doping on the electrical and catalytic properties of powder titania under UV and visible illumination, Chem. Phys. Lett. 6 (1984) 618–622.

[10] S. Alfred, U. Adriana, Electronic study of doping TiO_2 catalysts. 2. Doping with higher valence ions (WO_3) and variable valence ions (Cr_2O_3), Prog. Catal. 12 (1) (2003) 51–69.

[11] L.W. Richards, in: T.C. Patton (Ed.), Pigment Handbook, vol. 3, Wiley-Interscience, 1973, p. 93.

[12] A. Pathak, S. Mohapatra, S. Mohapatra, S.K. Biswas, D. Dhak, N.K. Pramanik, A. Tarafdar, P. Pramanik, Preparation of nanosized mixed-oxide powders, Am. Ceram. Soc. Bull. 83 (8) (2004) 9301–9306.

[13] S.B. Qadri, E.F. Skelton, D. Hsu, A.D. Dinsmore, J. Yang, H.F. Gray, B.R. Ratna, Size induced transition-temperature reduction in nanoparticles of ZnS, Phys. Rev. B 60 (13) (1999) 9191–9193.

[14] R.A. Spurr, H. Myers, Quantitative analysis of anatase–rutile mixtures with an X-ray diffractometer, Anal. Chem. 29 (1957) 760–762.

[15] A.R. West, Solid State Chemistry and its Applications, John Wiley and Sons, New York, 1984, pp. 368.

[16] A.S. Marfunin, Physics of Minerals and Inorganic Materials, Springer-Verlag, Berlin Heidelberg, New York, 1979, p. 340.

[17] A.B.P. Lever, Inorganic Electron Spectroscopy, Elsevier, Amsterdam, 1968.

[18] R.M. Johnston, in: T.C. Patton (Ed.), Color Theory, In Pigment Handbook vol. III, Wiley-Interscience, 1973, pp. 229–288.